

# Effective Reduction of Horizontal Error in Laser Scanning Information by Strip-Wise Least Squares Adjustments

---

Byoung Kil Lee, Kiyun Yu, and Moowook Pyeon

**Though the airborne laser scanning (ALS) technique is becoming more popular in many applications, horizontal accuracy of points scanned by the ALS is not yet satisfactory when compared with the accuracy achieved for vertical positions. One of the major reasons is the drift that occurs in the inertial measurement unit (IMU) during the scanning. This paper presents an algorithm that adjusts for the error that is introduced mainly by the drift of the IMU that renders systematic differences between strips on the same area. For this, we set up an observation equation for strip-wise adjustments and completed it with tie point and control point coordinates derived from the scanned strips and information from aerial photos. To effectively capture the tie points, we developed a set of procedures that constructs a digital surface model (DSM) with breaklines and then performed feature-based matching on strips resulting in a set of reliable tie points. Solving the observation equations by the least squares method produced a set of affine transformation equations with 6 parameters that we used to transform the strips for adjusting the horizontal error. Experimental results after evaluation of the accuracy showed a root mean squared error (RMSE) of the adjusted strip points of 0.27 m, which is significant considering the RMSE before adjustment was 0.77 m.**

## I. INTRODUCTION

Current technological advances in airborne laser scanning (ALS) enable it to successfully replace traditional methods for generating digital elevation models (DEM) [1]. ALS has several advantages in making a DEM, such as reduced costs and labor intensity, promptness, and potential for high geometric accuracy. Due to these advantages, the technique has quickly spread to other applications, including generating digital surface models (DSMs), constructing 3-D digital city models [2], [3], and automatically compiling building boundaries even when the buildings have many breaklines on their roofs [4].

Though the technique shows many advantages in terrain mapping, there remains some margin to further improve its geometric performance [5]. Research by Baltasvias [6] showed that the geometric accuracy level of ALS is about 20 cm in the horizontal plane and  $H/1000$  in the vertical plane, with  $H$  representing the flying height above ground. Considering an airplane's normal flying height, the level of accuracy by ALS in the horizontal plane is relatively low compared to that in the vertical plane. Advancement in techniques for enhancing horizontal accuracy is required to enable use of this technique on such applications as route surveying and precise topographical mapping. This is particularly true when the required scale of the topographic maps is large (e.g., there are 78 cities and towns in Korea for which 1:1,000 scale topographic maps must be created and regularly updated). This improvement will require inventing better techniques for data acquisition and post-processing of scanned data.

With this increased need to enhance ALS horizontal

---

Manuscript received Feb. 16, 2002; revised Feb. 4, 2003.

Byoung Kil Lee (phone: +82 2 446 1500, e-mail: basil@tastech.co.kr) is with TAS Tech Co., Ltd., Seoul, Korea.

Kiyun Yu (e-mail: kiyun@snu.ac.kr) is with Seoul National University, Seoul, Korea.

Moowook Pyeon (e-mail: neptune@konkuk.ac.kr) is with Konkuk University, Seoul, Korea.

accuracy, a series of studies have been performed in recent few years. One avenue of investigation was an effort to enhance scanner precision by upgrading its mechanics, but this only provided a slight improvement when compared with its cost. Other investigators have tried to reduce the error level by developing algorithms to post-process the scanned data. Research by Kraus and Pfeifer [7] showed there are considerable systematic differences between strips of data in the same area. This was found from observing minute undulations of contours from different strips. Huising and Gomes Pereira [8] also reported similar results, indicating the importance of strip-wise adjustment. Paying correct attention to the flight path and corresponding scanning patterns of the ALS revealed that there were systematic errors between strips of data on different paths.

Among the efforts to address this error problem, experiments at the Institute of Photogrammetry of Stuttgart University in Germany and Delft University of Technology in The Netherlands are noteworthy. They used matching results of a DEM for adjusting 3-D models of scanned strip data. Due to difficulties in matching a rasterized DEM caused by the ambiguity and discontinuity inherent in 3-D data points, however, results were not satisfactory and needed further refinement [9]-[11]. On the other hand, research of Rijkswaterstaat in The Netherlands has focused on correcting errors in vertical values with the bundle block adjustment method [12].

Considering the importance of this issue, this article focuses on reducing systematic differences of strip data from different paths that cause errors and on developing an effective algorithm to adjust the differences while ignoring other possible sources of minor errors. Our analysis consisted of four phases. The first step looked at the systematic differences of strip data that strongly rely on some mechanical limit of the ALS system. With the help of several experiments [9], [11], we identified and summarized the possible error sources and their sizes in systematic and random terms. From the resulting understanding, in the next step, we set up an observation equation to adjust the differences between strip points. Looking at a pair of strips as a stereo model in aerotriangulation, we matched and registered the strips to the ground in a manner resembling successive orientation and absolute orientation. This adjustment, which is called "pass adjustment," aims at reducing the errors of the data points in an entire range by adjusting differences between strips and decreasing discrepancies between each data position and its corresponding ground reference. In the next step, we developed and proposed a set of procedures to extract a DSM. Extracting a DSM of good quality was important because features such as building boundaries were identified and used for matching the strips,

which then enabled us to generate a set of tie points in the strips. These points were necessary for setting up the observation equations. In generating the DSM, the raw ALS data points were rasterized. To reduce the introduction of errors, we skipped the interpolation normally used in rasterization, and rather, adopted a series of alternative processes in the proposed algorithm. The output DSM clearly saved the breaklines. In addition to the tie points, a number of control points were also necessary for completing the observation equations. Finally, we selected a number of control points identifiable on both the DSM and aerial photos and used them to complete the equations. After setting up the observation equations, we solved them with a least squares method. This process developed a set of affine transformation equations in the x and y directions. Using these transformation equations, we were able to transform, i.e., adjust, all data points on the strips. The last part of this article describes our evaluation of the adjusted strips, in which we measured and compared the coordinates of building corners from both the adjusted strips and aerial photos. We followed the evaluation with a hypothesis test.

## II. ERROR IN THE AIRBORNE LASER SCANNING SYSTEMS

Mechanically, the ALS system consists of a laser scanner, a global positioning system (GPS) antenna and receiver, and an inertial measurement unit (IMU). A ranging unit and scanner that are integrated and controlled by a control unit make up the laser scanner. The system determines horizontal (x, y) and vertical (z) coordinates of points on the ground's surface, while the GPS measures the sensor's position, the IMU measures the sensor's attitude, and the laser scanner measures the distance between the ground surface and the scanner, including its direction. The scanned point's density, as well as other characteristics of the data points, depends on the scanning angle, scanning rate, flying height, platform velocity, and scanner measuring frequency [1].

As the complex characteristics of these data points imply, there are various causes and sizes of errors in the scanned data points. According to Crombagh et al. [12], errors in ALS can be classified into four groups: error per block, error per strip, error per GPS observation, and error per point. Other approaches, particularly by Huising and Gomes Pereira [8], tried to explain these errors in systematic and random terms by conducting some field verification experiments. From these studies, we summarized the magnitudes and causes of possible errors of the ALS in Table 1. These errors influence both the relative accuracy between strips and the absolute accuracy with respect to the ground reference.

Among these sources of error, the one from the IMU is of

particular concern, as systematic differences on strips depend strongly on the error from the IMU [8], [9]. Table 1 shows that errors from the IMU comes from its drift during scanning. On one flight path, the drift of the IMU consistently increased or decreased by an amount up to  $0.04^\circ$  in the x and y directions and  $0.08^\circ$  in the z direction. This drift of the scanner plays a role, producing significant systematic differences in strips while scanning the same ground surface. Developing techniques to adjust these errors would be an important means for enhancing horizontal accuracy.

Table 1. Possible ALS error sources and their sizes.

Error Source	Size of Systematic Term	Size of Random Term
GPS(X,Y,Z)	Depends on reference station, ionosphere & troposphere	$\pm 0.1$ m
Distance Measurement	Depends on weather condition (temperature, humidity, etc.)	$\pm 0.1$ m
IMU( $\omega, \varphi$ )*	Drift: up to $0.04^\circ$	Noise: $0.01^\circ$
IMU( $\kappa$ )*	Drift: up to $0.08^\circ$	Noise: $0.01^\circ$

\*typical value of the ALTM series of Optech, Inc. [6]

### III. OBSERVATION EQUATIONS FOR STRIP-WISE ADJUSTMENTS

As stated earlier, the IMU is one of the main causes of horizontal error in scanned data points and errors very often increase or decrease with consistency in a flight's direction. This error consistency implies a linear relationship. Kilian et al. [9] developed a model to adjust the error using 12 parameters. These parameters indicate the initial values of positional and attitude error. Also indicated is their variance with time change. Kilian et al.'s [9] mathematical model is

$$dX(t) = \Delta X(t_0) + v_x(t) + f((\Delta\omega(t_0) + v_\omega(t)) + (\Delta\varphi(t_0) + v_\varphi(t)) + (\Delta\kappa(t_0) + v_\kappa(t))) \quad (1)$$

$$dY(t) = \Delta Y(t_0) + v_y(t) + f((\Delta\omega(t_0) + v_\omega(t)) + (\Delta\varphi(t_0) + v_\varphi(t)) + (\Delta\kappa(t_0) + v_\kappa(t))) \quad (2)$$

where  $\Delta X(t_0)$ ,  $\Delta Y(t_0)$  indicate the initial position error by the GPS,  $\Delta\omega(t_0)$ ,  $\Delta\varphi(t_0)$ ,  $\Delta\kappa(t_0)$  indicate the initial attitude error by the IMU,  $v_x(t)$ ,  $v_y(t)$  indicate the position error along the time change, and  $v_\omega(t)$ ,  $v_\varphi(t)$ ,  $v_\kappa(t)$  indicate the attitude error along the time change.

This model shows that the error in a point relies heavily on the drift of the IMU and error of the GPS unit. In such point

errors, some portions contribute to the systematic differences between strips. Because the systematic differences are linear, an appropriate transformation equation might help account for the differences. Such a transformation equation could be in linear conformal form or in affine form with 6 parameters. In some cases, an 8 parameter affine form could be useful because it might account for some minor non-linear components. One more factor to consider in selecting an appropriate transformation equation is the feasible number of tie points and control points in the strips. To correct a set of strips simultaneously requires two observation equations—one for control points and another for tie points—as with the bundle adjustment. The observation equation for the control points of each strip is

$$A_{ij}p_j = D_{ij}, \quad (3)$$

where  $A_{ij}$  is the coefficient matrix of the  $i$ -th control point on the  $j$ -th strip,  $p_j$  is the unknown coefficient of the transformation equation on the  $j$ -th strip, and  $D_{ij}$  is the discrepancy in the control point coordinates between the measured and ground references. The observation equation for the tie points, assuming their coordinates are unknown, is set up as

$$A_{ij}p_j - IX_i = 0, \quad (4)$$

where  $X_i$  is the adjusted values of the  $A_{ij}$ . Using these relationships, equations for correction in the x and y directions for each data point are calculated to adjust the raw ALS data.

### IV. GENERATION OF THE DIGITAL SURFACE MODEL AND MATCHING

If the DSM has clear breaklines generated from the raw data points, then it is possible to extract a set of tie points by DSM matching, as well as control points in the strips. The observation equations can be completed and solved using the coordinates of these points.

We used a methodological approach to find algorithms effective in obtaining matching points and control points in strips. Rather than focusing on deriving identifiable surface features and using them for matching in these algorithms, we used each rasterized cell value on corresponding neighbor strips for comparison in matching. Behan [10] used a Foerstner operator to obtain candidate points for matching and ran least squares matching for  $15 \times 15$  neighbor cells. However, the results were not sufficiently satisfactory, so he used manual selection of matching points instead. He attributed the unsatisfactory results to erroneous distortions that occurred

during interpolation in rasterization of the irregularly spaced raw data. These distortions were influenced mainly by occlusion in addition to inappropriate grid size and binning error. To reduce such distortions, Maas [13] built a triangular irregular network (TIN) and used roofs over other features for matching. This was done to exclude the deleterious effects of occlusion and random error from grass land. This method is, however, still not satisfactory for simple roofs, such as flat and gabled roofs that induce singularity. In addition, other problems, such as errors in data points, diverse structures of roofs, sizes of laser footprints, and low density of data points, also lower matching accuracy. Due to these unsatisfactory results, other methods are needed, such as comparing parameters of objects (e.g., buildings or roof planes) or utilizing additional information (e.g., laser reflectivity).

To avoid the problems in previous investigations to some extent, this research adopted step-wise feature-based matching. For this kind of matching, we proposed an algorithm to construct a DSM with breaklines. Our algorithm used a set of filtering methods rather than interpolation to suppress the deleterious effects of occlusion and some other factors and to detect breaklines as clearly as possible. This method made effective extraction of features possible. One more reason for adopting step-wise feature-based matching is to avoid singularity in matching. In TIN-based matching, flat roofs—and sometimes even gabled roofs—induce singularity because the surface gradients are not easy to discern on two different templates of the same roof. This is particularly true in our test area, in which the majority of roofs are flat due to the architectural tradition of the region. The following section explains the step-wise feature-based matching in detail.

Feature-based matching requires capturing surface features that can be compared to getting matching points. Deciding on the type of surface features to capture involves determining what attributes of the features are to be used. Buildings and building boundaries are selected because corners or sides of buildings usually provide high contrast height values against their neighbors. It's hard to determine exact corner points from characteristics of the ALS data points (i.e., irregular scattering with some intervals), and in reality they may have random errors with a size of half the average point interval. The centers of gravity of buildings rather than the corner points are therefore preferable. The centers provide several advantages over the corner points: (1) more chances to eliminate random errors of corner points, (2) higher relevance to not-in-square buildings, and (3) reduced errors from rasterization. Thus, we chose to use centers of gravity for matching.

Capturing building boundaries involve two steps: first segment building areas and then label them. Segmentation of building areas is possible with a geomorphological filter or

local maxima histogram [14]. The geomorphological filter has the advantage of a reduced elapsed time, while the local maxima histogram reduces deformations during rasterization of raw data points. Clear definition of the building segment is difficult with both of these methods, because during the rasterization process interpolation introduces problems of ambiguous breaklines [10]. To partially solve this problem, Behan [10] adopted nearest neighbor binning. This solution was limited because deformation is not fully addressed by the interpolation process when it fills cells without the values caused by occlusion and irregularity of raw data points. Thus, it was of critical concern to develop a more suitable algorithm for determining building segments with reduced deformation. The key to developing such an algorithm was to address the question of how to save breaklines so as not to blur the building boundaries. We propose an algorithm to meet this need. First, we generated a null DSM and filled it by employing a local maxima filtering concept and then applied a selective maxima/minima filter to fill cells without the height values due to occlusion and irregularity of raw data points.

To generate the null DSM, we created a DSM with no value cells. To decide on the null DSM interval, we had to consider the ALS scanning pattern. The scanning pattern showed that the scanner drew a zigzag footprint on the ground and that there were increasing intervals between data points as the scanning angle was repositioned further from the nadir. Too large an interval induced a loss of data points, whereas an interval too small induced too many null cells, and these could not be replaced with other values later in the process. Thus, we selected an integer near to the mean distance between laser points for an appropriate cell interval. Before filling up the null DSM, we checked points of blunders using a threshold and eliminated any point whose value exceeded this threshold. After completing the null DSM, we applied the local maxima filter. Next, we went on to the process of replacing the null DSM cell values with values reflecting ground surface features. The null DSM was overlaid on the data points for cell-wise checking to determine whether there were corresponding data points within each cell. If the number of corresponding data points was one, then its value replaced the null cell. If there were more than one point, then the highest among the multiple values was used in the cell. Multiple points imply that multiple data points can exist in the same cell (i.e., when the ALS scans a side of a building, there are some return signals from concrete walls and other return signals from ground layers after the laser pulses pass through a window). In this case, we assumed that the highest value indicated the building height and we selected this value for the cell replacement.

Although many null cells were replaced with proper surface feature values through this process, some null cells were still

not replaced. We put these cells through a series of comparisons to find relevant replacements. At first, a moving window of three cells by three cells was introduced and its center was put on each null cell. Then, eight neighbor values of the null cells were examined, and the null cell qualified for replacement only if there were more than four neighbor cells already replaced; otherwise it remained a null cell. This was necessary to avoid interpolation when point density of the raw data was too low, or there were occlusions. This was done so that no influence was introduced by local deformations due to extensive interpolation. Next, the difference between the maximum and minimum values from the eight neighbor cells were calculated and checked to see if it exceeded a certain threshold. If it was below the threshold, the mean of the eight neighbor cell values was assigned as the replacement value.

The threshold value was determined by using the lowest building height in the strip and it was selected on the basis of a field survey. This process judges whether there were buildings within the window, and if there were buildings, another comparison was required to decide whether the null cell belonged to the building area. The last comparison determined whether or not the null cell was in a building. If the number of cells larger than the mean of eight neighbors was more than or equal to four, the null cell was replaced with the maximum, assuming the null cell was in the building. Otherwise, the null cell was replaced with the minimum, assuming the null cell was not in the building. All sequences for generating the DSM are shown in Fig. 1.

To this point, we have presented an algorithm to generate a DSM for effective segmentation of building areas. The next

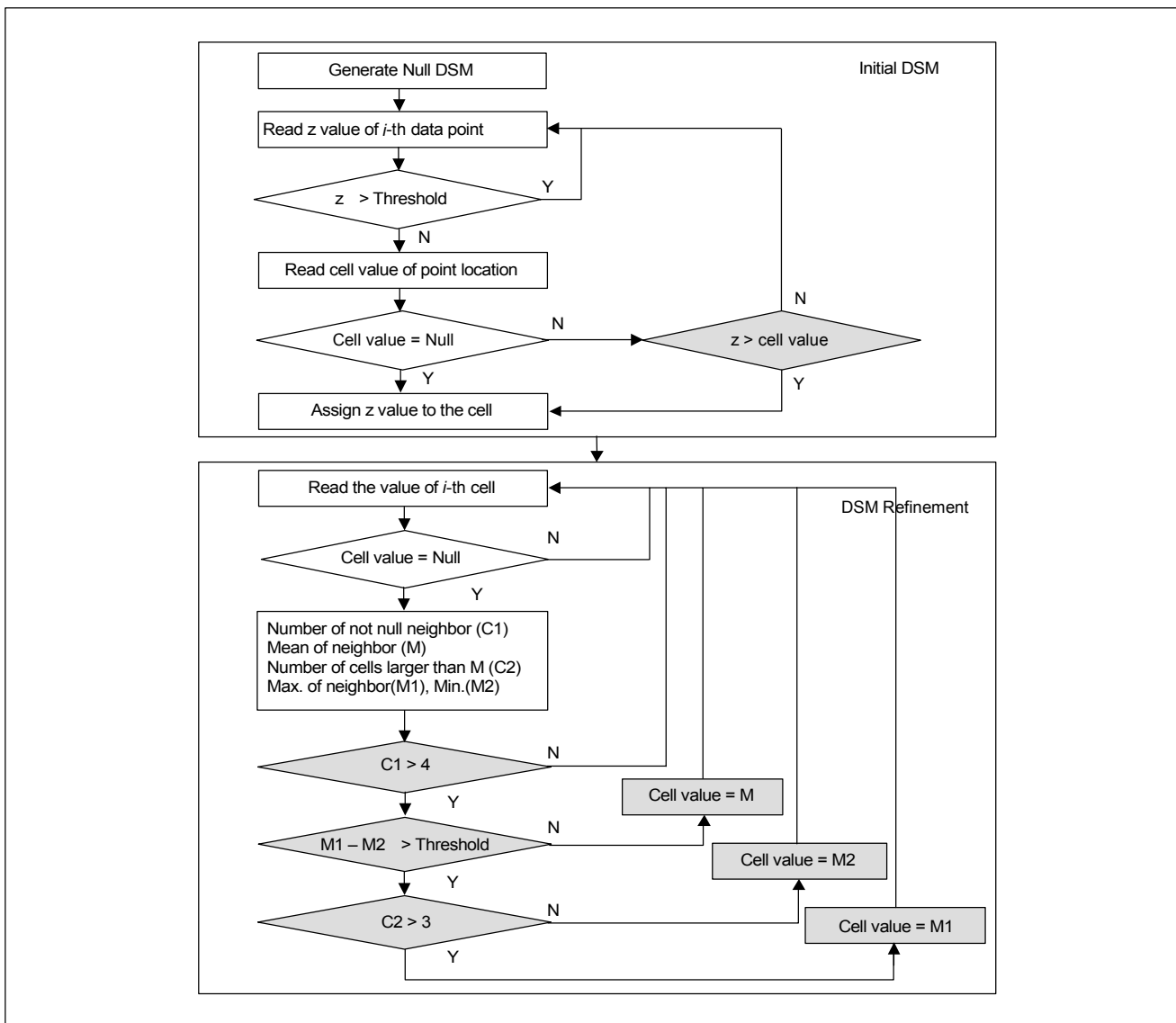


Fig. 1. DSM generation algorithm for effective segmentation of building areas.

step segmented and labeled the building areas. Segmentation of the building areas was done by the geomorphological method that proved valid for the DSM by Cha et al. [15] and Maas and Vosselman [14] (Fig. 2(a)). For labeling, a unique ID was assigned to the points in one building area so that these points could be identified as constituents of a building area. From the labeled points in a building area, a polygon was generated and coordinates of the gravity center of the polygon and corresponding area were calculated for matching strips (Fig. 2(b)).

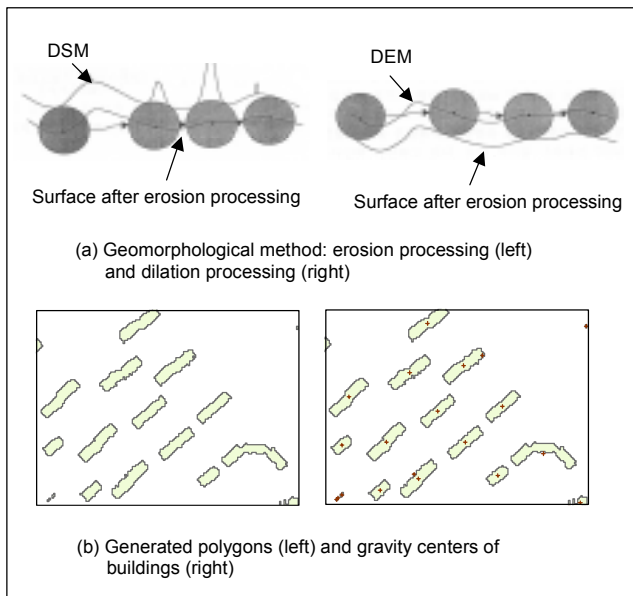


Fig. 2. Segmenting building areas and labeling them. (a) a geomorphological opening operation consists of erosion followed by dilation to extract a DEM from the DSM. Subtraction of the DEM from the DSM allows segmentation of the building areas. (b) generated polygons and corresponding labels at gravity centers.

## V. DATA ACQUISITION AND ANALYSIS

For testing, we selected an area spanning Soonae-Dong and Jungga-Dong, parts of the City of Bundang, located about 19 km south of downtown Seoul. Scanning was done using an ALTM1020 from Optech in Canada on a PA31-350 platform in March 2000. A total of 28 scans were performed along different flight paths, 14 in the morning and 14 in the afternoon. Of these 28, we selected four for testing as they covered the entire test site with appropriate overlap. Table 2 contains the detailed information regarding the overlap ratio, flying velocity, and scan angle. The dimension of the scanning coverage was 800 m by 800 m on the ground, on which surface features such as buildings, roads, and grass are well distributed. The mean point interval was 1.82 m along the scan direction and 1.78 m

along the flight direction. Figure 3 shows the test site of the scanned data points. As tools for processing the data at each stage, Visual C++ of MicroSoft, ArcInfo, and ArcView of ESRI were used.

Table 2. Technical specification of scanner systems.

Flying height (m)	800
Flying velocity (km/h)	230
Repetition rate (Hz)	5,000
Scan angle (°)	±9
Swath width (m)	253
Overlapping ratio (%)	30 – 70
Scan rate (Hz)	18
Point density (points/m <sup>2</sup> )	0.31



Fig. 3. Test site of the scanned data points showing different strips with different tones.

The proposed algorithm with the scanned data points generated DSMs with 2 m resolutions. The interval was chosen to be the closest integer to the mean of the raw data interval along the scan and flight directions. When the DSM was generated, two thresholds were chosen: one for eliminating blunder data points and the other for deciding whether there were buildings in the moving window. For eliminating blunder data points, a range higher than the highest surface feature and lower than half of the flying height was chosen. Values in this range are likely to be blunders because they are not feasible values for the test site. For checking the existence of buildings

in the moving window, a value of 10 m, was selected from a field survey. This value was higher than the lowest building height. If the difference of the local maximum and local minimum in the moving window was over 10 m, there were buildings in the window. After running the local maxima filter and the moving window to replace the null cells, we found significant differences between the DSM before running the moving window and the DSM afterwards (Fig. 4).

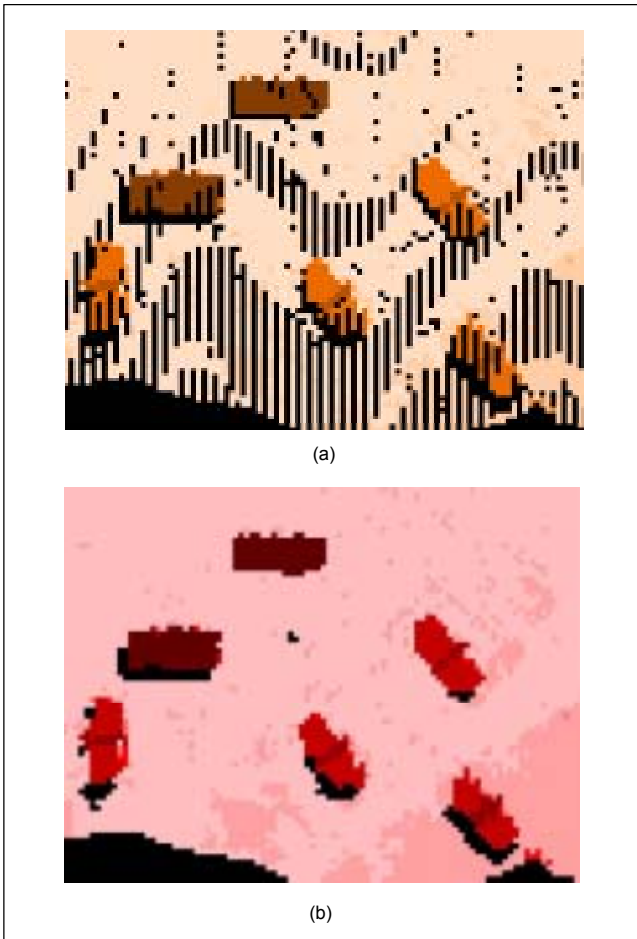


Fig. 4. Comparison of the DSM: (a) the DSM before running the moving window, (b) the DSM after running the moving window to replace the remaining null cells.

The DSM before running the moving window contains many strips of null cells along the scan direction. These null cells increased as the scan angle increased, whereas the DSM after running the moving window showed few null cells with clear breaklines on building boundaries.

From the DSM, we segmented and labeled the building areas and calculated the horizontal coordinates of the center of gravity for each segment. These points with horizontal coordinates, so called “candidate points” that do not really exist in the data file, were recorded in text format and used in

matching the strips. Actual matching consisted of a process to find points on two adjacent strips. For this, the candidate point locations and areas of corresponding polygons were compared on the two adjacent strips. Points with fewer locational and area differences were preferred. After this comparison, 5 points per strip, a total selection of 15 for 4 strips was made manually (Fig. 5). These matched points are the tie points between strips (Table 3). At this point, it is necessary to think about the geometric precision and homogeneity of the tie points because the proposed adjustment method depends on them. If they are significantly bad, adjusting the points with this method does not produce good results. Especially, if they are bad enough to overwhelm the systematic error from the drift of the IMU, the resulting point accuracy may not be enhanced after adjustments.

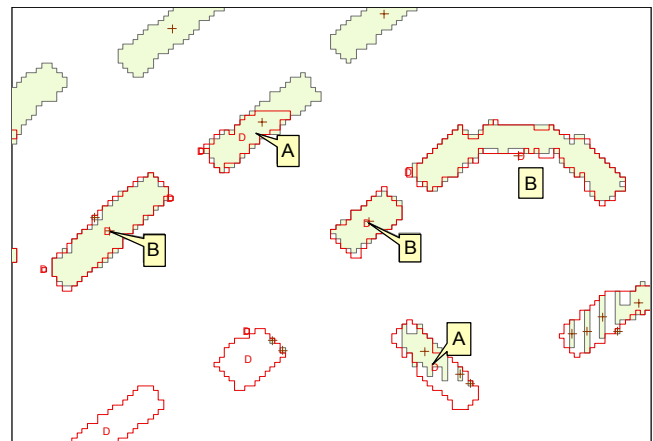


Fig. 5. Examples of selected and unselected candidate points. Points labeled “A” are examples of unselected points, rejected due to significant differences in point locations and the corresponding area, whereas points labeled “B” are examples of selected candidate points.

In addition to tie points, the coordinates of the control points are also required to complete the observation equations. With the DSM overlaid on the raw data points, we selected 7 corner points of easily identifiable buildings. To determine the corresponding ground coordinates, we manually located the same points on maps with a scale of 1:1,000 made from the aerial photos (Table 4). The aerial photos were taken on December 1999 with a scale of 1:5,000, a focal length of 153.59 mm, a flying height of 880 m, an exposure time of 1 pm, and an overlap of the end of 60% and the side of 30%.

Once we set up the observation equations, we solved them by the least squares method for a linear conformal transformation and an affine transformation of 6 parameters and 8 parameters. The results showed that the affine transformation of 6 parameters produced the least RMSE of 0.11 m and an  $S_0$  of 0.21 m, while the affine of 8 parameters had an RMSE of 0.14 m and an  $S_0$  of 0.23 m, and the linear

Table 3. Selected tie points and their coordinates by matching the strips.

Point id	X-Coord. (m)	Y-Coord. (m)	X-Coord. (m)	Y-Coord. (m)
	Strip 1		Strip 2	
8	332947.06	4137644.50	332947.88	4137645.75
11	332822.97	4137614.00	332824.75	4137614.25
16	333540.78	4137556.25	333541.19	4137557.75
21	332958.25	4137543.25	332957.91	4137544.25
22	333183.44	4137543.00	333183.78	4137544.00
	Strip 2		Strip 3	
23	333099.75	4137754.00	333099.63	4137753.50
26	332954.50	4137730.00	332954.19	4137728.50
27	333041.91	4137726.00	333041.50	4137725.00
30	333462.41	4137720.75	333462.13	4137719.50
33	333443.59	4137697.25	333442.44	4137697.00
	Strip 3		Strip 4	
35	332978.81	4137938.00	332980.56	4137938.00
36	333048.19	4137928.25	333048.44	4137928.75
41	333195.06	4137905.75	333196.09	4137906.50
42	333571.34	4137893.75	333572.25	4137894.75
47	333195.63	4137858.75	333196.09	4137858.25

Table 4. Selected control points and their coordinates.

Point id	Data Coordinate of Control Points		Ground Coordinate of Control Points	
	X-Coord.(m)	Y-Coord.(m)	X-Coord.(m)	Y-Coord.(m)
Control Points in Strip 1				
10001	333373.61	4137477.31	333373.23	4137478.1
10002	333415.64	4137513.41	333415.58	4137513.87
Control Points in Strip 2				
10003	333250.77	4137511.26	333250.44	4137510.55
10004	333339.49	4137507.92	333338.56	4137507.48
10005	333376.79	4137542.53	333376.07	4137541.74
Control Points in Strip 3				
10006	333179.96	4137886.8	333180.5	4137887.43
Control Points in Strip 4				
10007	333110.94	4137969.23	333111.28	4137969.81

conformal had an RMSE of 0.16 m and an  $S_0$  of 0.25 m, where RMSE is the root-mean-square of the coordinate residuals and  $S_0$  indicates the reference standard deviation from the least

squares adjustment. Considering the shear on the data points from the drift of the IMU, the affine transformation may be expected to produce better results than the linear conformal one.

The independence of rotation of the IMU in the x, y, z directions means that there is no need to consider the (x, y) term in the affine transformation so the 6 parameter transformation, rather than the 8, may produce better results. Accordingly, we selected the affine transformation with 6 parameters for the adjustment of the horizontal coordinates of the data points on strips. The resulting equations for each strip are

$$\begin{aligned} \text{for strip 1} \quad dX &= -0.52730 - 0.00105x + 0.00121y \\ dY &= 3.48074 + 0.00232x - 0.00797y, \end{aligned} \quad (5)$$

$$\begin{aligned} \text{for strip 2} \quad dX &= -2.16434 - 0.00135x + 0.00390y \\ dY &= -0.99435 + 0.00232x - 0.00050y, \end{aligned} \quad (6)$$

$$\begin{aligned} \text{for strip 3} \quad dX &= 0.58155 - 0.00151x + 0.00017y \\ dY &= -7.57514 + 0.00285x + 0.00848y, \end{aligned} \quad (7)$$

$$\begin{aligned} \text{for strip 4} \quad dX &= 2.82810 - 0.00163x - 0.00231y \\ dY &= -3.96233 + 0.00265x + 0.00448y. \end{aligned} \quad (8)$$

To evaluate the accuracy of the adjusted strips, we compared the point coordinates in the strips with their corresponding values on the maps. A total of 12 identifiable points, usually corner points of buildings, were selected and their coordinates

were read on both the strips and maps. Then the differences of the coordinates in x (easterly) and y (northerly) directions were calculated. Comparison of these results indicated that the maximum difference reduced from 1.03 m in x direction before adjustment and 0.84 m in y direction before adjustment to 0.33 m in x direction after adjustment and 0.35 m in y direction after adjustment; the mean difference reduced from 0.51 m and 0.48 m to 0.16 m and 0.15 m; and the RMSE reduced from 0.56 m and 0.53 m to 0.19 m and 0.19 m, respectively (Table 5). The resulting accuracy of the points was close to the allowable error, i.e., an RMSE of 0.2 m and a maximum error of 0.4 m, for 1:1,000 digital maps specified by the National Geography Institute in Korea.

To examine whether the results were statistically significant, we conducted a hypothesis test. In this test, we examined the differences between the measurements before adjustment and after adjustment to determine if they were significantly large from a statistical point of view. We set up the test statistic as follows:

$$T = \frac{\bar{X}_b - \bar{X}_a}{S_p \sqrt{\frac{1}{n_b} + \frac{1}{n_a}}}, \quad (9)$$

Table 5. Comparison results of points before and after adjustment.

Point id	Reference		Before Adjustment				After Adjustment			
	X (m)	Y (m)	X (m)	dX (m)	Y (m)	dY (m)	X (m)	dX (m)	Y (m)	dY (m)
1	333110.26	4137528.34	333110.85	-0.59	4137529.05	-0.71	333110.53	-0.27	4137528.02	0.32
2	333149.79	4137560.23	333150.45	-0.66	4137561.00	-0.77	333149.80	-0.01	4137560.05	0.18
3	333250.50	4137510.57	333250.61	-0.11	4137511.10	-0.53	333250.28	0.22	4137510.40	0.17
4	333376.08	4137541.76	333377.11	-1.03	4137542.60	-0.84	333376.41	-0.33	4137542.03	-0.27
5	333415.56	4137513.90	333415.99	-0.43	4137514.25	-0.35	333415.69	-0.13	4137513.88	0.02
6	333293.54	4137742.24	333293.34	0.20	4137742.49	-0.25	333293.65	-0.11	4137742.15	0.09
7	333221.97	4137839.54	333221.51	0.46	4137838.91	0.63	333222.13	-0.16	4137839.51	0.03
8	333349.61	4137896.55	333348.74	0.87	4137896.09	0.46	333349.64	-0.03	4137896.64	-0.09
9	333287.91	4137846.59	333287.49	0.42	4137846.47	0.12	333287.63	0.28	4137846.60	-0.01
10	333175.33	4137874.28	333174.91	0.42	4137873.85	0.43	333175.28	0.05	4137873.93	0.35
11	333201.11	4137901.43	333200.63	0.48	4137901.17	0.26	333201.18	-0.07	4137901.67	-0.24
12	333180.51	4137887.44	333180.10	0.41	4137886.97	0.47	333180.31	-0.20	4137887.38	0.06
Mean dX or dY (m)			0.51		0.48		0.16		0.15	
Maximum dX or dY (m)			1.03		0.84		0.33		0.35	
RMSE (m)			0.56		0.53		0.19		0.19	
RMSE (m) in position			0.77				0.27			

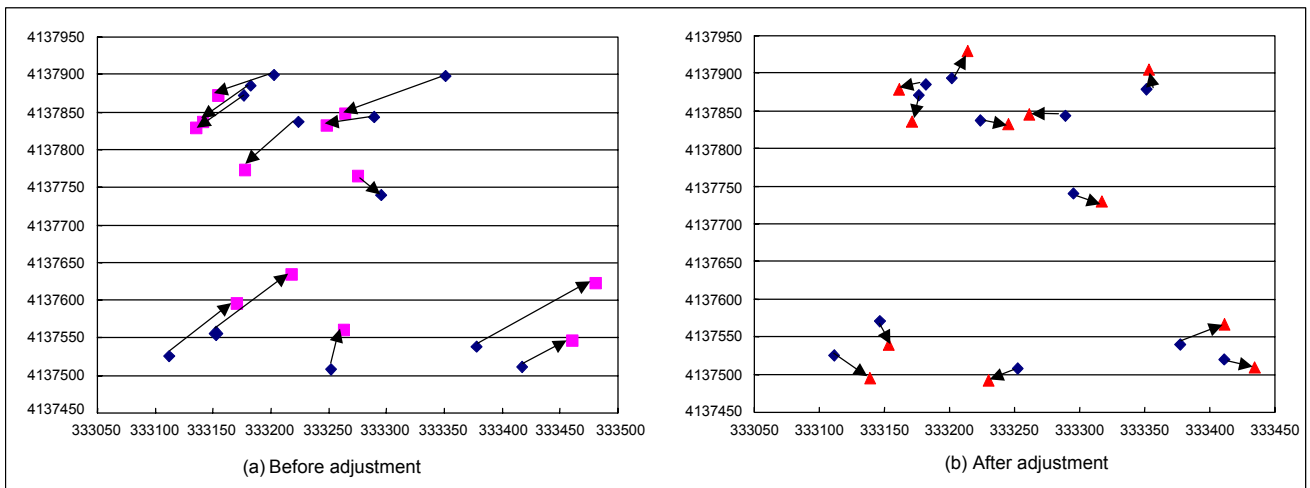


Fig. 6. Difference vectors for 12 check points (magnified by  $\times 100$ ): (a) before adjustment, (b) after adjustment.

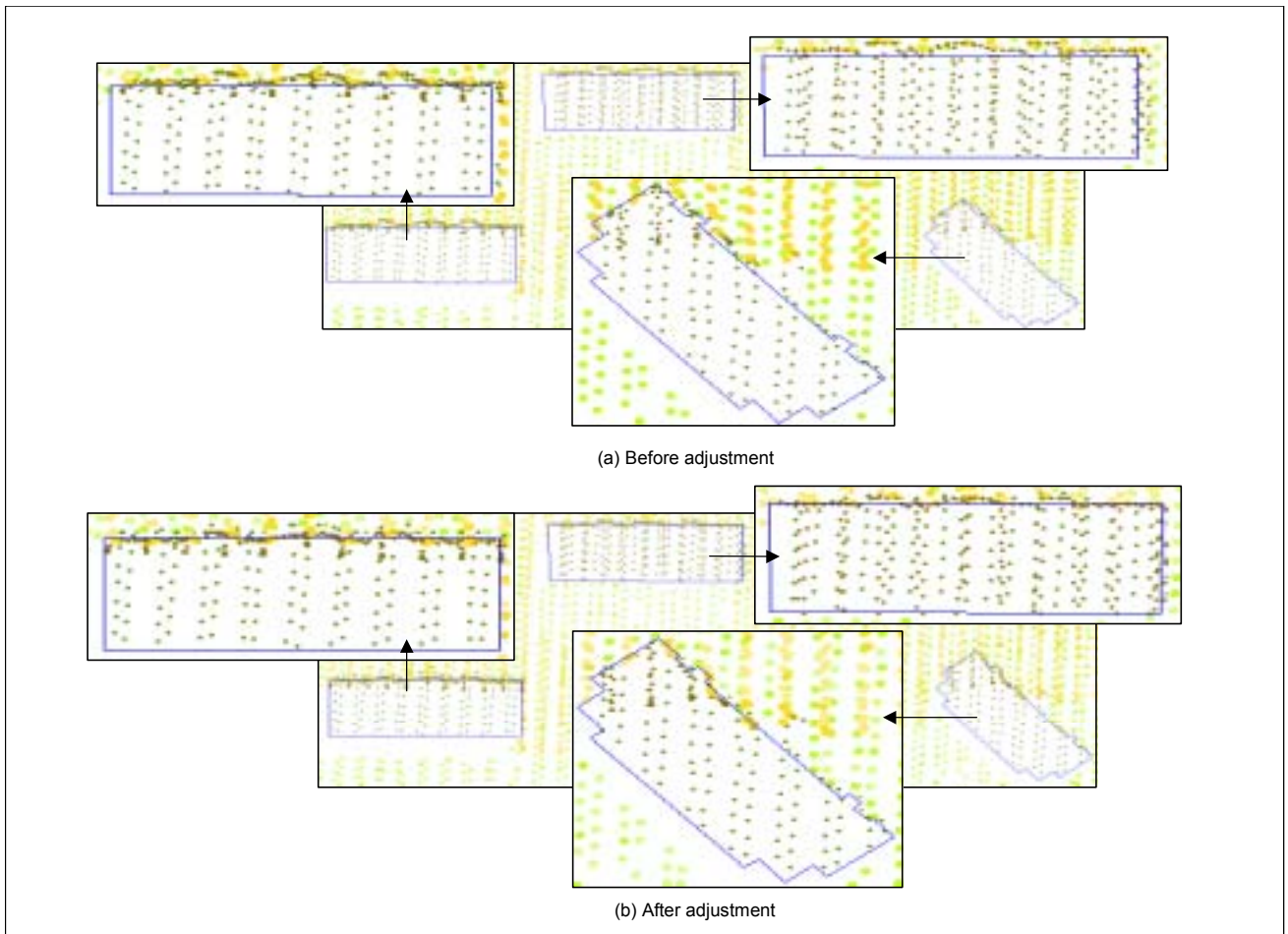


Fig. 7. Overlay of building boundaries on strips: (a) before adjustment, (b) after adjustment.

where  $S_p = \frac{(n_b - 1)S_b^2 + (n_a - 1)S_a^2}{n_b + n_a - 2}$  indicates the pooled standard deviation,  $n_b$ ,  $\bar{X}_b$ ,  $S_b$  indicate the number of

control points, the mean difference in the x direction, and the standard deviation of differences before adjustment, and  $n_a$ ,  $\bar{X}_a$ ,  $S_a$  indicate the number of control points, the mean

difference in the x direction, and the standard deviation of differences after adjustment. The corresponding null hypothesis was  $H_o: \bar{X}_b \leq \bar{X}_a$ , and the rejection region was  $T > t(n_b + n_a - 2, \alpha)$ . The test result yielded a  $t$  value of 4.900 in the x direction and 5.084 in y the direction, which rejects  $H_o$  at  $\alpha=99\%$  ( $t=2.508$ ). This result implies that the error in the data points after adjustment was reduced by a statistically significant amount.

Figure 6 shows the difference vectors in the x-y plane before (a) and after (b) adjustments, where the abscissa indicates x and the ordinate indicates y. For visual comparison of the point accuracy before and after adjustments, building boundaries from the maps were extracted and overlaid on the strips (Fig. 7). These figures also verify that the points' errors were reduced after adjustment.

## VI. SUMMARY AND CONCLUSIONS

In our investigation, we developed an algorithm to adjust ALS data points and applied it to a test site. We set up observation equations and proposed an algorithm for effectively deriving tie and control points. Solving these equations using the least squares method, we generated a set of affine transformation equations with 6 parameters for transformation of each strip. Experimental results showed that the positional RMSE of the transformed data points decreased from 0.77 m (before adjustment) to 0.27 m (after adjustment). A hypothesis test revealed that the decrease of the RMSE after the adjustment was statistically significant. However, we concede that the results are from a relatively small test site and it is still not certain whether the results are representative of other cases. Though caution should be exercised in using them, these results seem very promising. With respect to using the data for 1:1,000 scale mapping in Korean cities, provided the algorithm allows a similar RMSE as the one of our test site, one can expect the resulting accuracy to be very close to the national accuracy specification in these cities due to the similar architectural tradition.

With the other benefits of reduced cost and promptness, the enhanced accuracy potential of the ALS technique might make it popular in many other applications. Nevertheless, there is still a large margin for improvement. We need to develop methods to effectively capture the tie and control points when few artificial surface features, e.g., buildings or roads, exist. In the long term, studies to identify the exact causes and corrections of scanner errors might be useful.

## ACKNOWLEDGEMENT

The authors wish to thank the Korea Research Foundation and Institute of Engineering Science at Seoul National University for their support.

## REFERENCES

- [1] A. Wehr and U. Lohr, "Airborne Laser Scanning-an Introduction and Overview," *ISPRS Journal of Photogrammetry and Remote Sensing*, vol. 54, 1999, pp. 68-82.
- [2] Jongchan Lee, Byung-Han Ryu, and Jeehwan Ahn, "Estimating the Position of Mobiles by Multi-Criteria Decision Making," *ETRI J.*, vol. 24, no. 4, Aug. 2002, pp. 323-327.
- [3] Byoung-Kil Lee, Yang-Dam Eo, Jae-Joon Jeong, and Yong-Il Kim, "A Cost Effective Reference Data Sampling Algorithm Using Fractal Analysis," *ETRI J.*, vol. 23, no. 3, Sept. 2001, pp. 129-137.
- [4] J.M. Hill, L.A. Graham, R.J. Henry, D.M. Cotter, D. Young, "Wide-Area Topographic Mapping and Applications Using Airborne Light Detection and Ranging (LIDAR) Technology," *PE & RS*, vol. 66, no. 8, 2000.
- [5] M.Y. Shin and C.H. Park, "A Radial Basis Function Approach to Pattern Recognition and Its Applications," *ETRI J.*, vol. 22, no. 2, 2000, pp. 1-10.
- [6] E.P. Baltsavias, "Airborne Laser Scanning: Existing Systems and Firms and Other Resources," *ISPRS Journal of Photogrammetry and Remote Sensing*, vol. 54, 1999, pp. 164-198.
- [7] K. Kraus and N. Pfeifer, "Determination of Terrain Models in Wooded Areas with Airborne Laser Scanner Data," *ISPRS Journal of Photogrammetry and Remote Sensing*, vol. 53, 1998, pp. 193-203.
- [8] E.J. Huising and L.M. Gomes Pereira, "Errors and Accuracy Estimates of Laser Data Acquired by Various Laser Scanning Systems for Topographic Application," *ISPRS Journal of Photogrammetry and Remote Sensing*, vol. 53, 1998, pp. 245-261.
- [9] J. Kilian, N. Haala, and M. Englich, "Capture and Evaluation of Airborne Laser Scanner Data," *IAPRS*, vol. 31/3, ISPRS, 1996, pp. 383-368.
- [10] A. Behan, "On the Matching Accuracy of Rasterised Scanning Laser Altimeter Data," *Int'l Archives of Photogrammetry and Remote Sensing*, vol. 33, Part B2, Amsterdam, 2000.
- [11] A. Behan, H-G. Maas, and G. Vosselman, *Step towards Quality Improvement of Airborne Laser Scanner Data*, [http://www.geo.tudelft.nl/fts/papers/2000/behant2000\\_quality.pdf](http://www.geo.tudelft.nl/fts/papers/2000/behant2000_quality.pdf), 2000.
- [12] M.J.E. Crombaghs, R. Brügelmann, and E.J. de Min, "On the Adjustment of Overlapping Strips of Laseraltimeter Height Data," *Int'l Archives of Photogrammetry and Remote Sensing*, vol. 33, Part B3, Amsterdam, 2000, pp. 230-237.
- [13] H. Maas, "Least-Squares Matching with Airborne Laserscanning Data in a TIN Structure," *Int'l Archives of Photogrammetry and Remote Sensing*, vol. 33, Part B3, Amsterdam, 2000, pp. 548-555.
- [14] H. Maas and G. Vosselman, "Two Algorithms for Extracting

Building Models from Raw Laser Altimetry Data,” *ISPRS Journal of Photogrammetry and Remote Sensing*, vol. 54, 1999, pp. 153-163.

- [15] Young-su Cha, Yong-il Kim, Yang-dam Eo, and Byoung-kil Lee, “A Study on the Extraction of Building for Three Dimensional City Model,” *Journal of the Korean Society for Geo-Spatial Information System*, vol. 3, no. 1, Mar. 1999, pp. 75-86.



**Byoung Kil Lee** received the BS and PhD degrees in GIS and remote sensing from Seoul National University in Korea in 2001. He is a CTO of TAS Tech Co., Ltd., one of the leading companies in Business GIS. He teaches GIS and RS in Hankyong National University as well.



**Kiyun Yu** received the BS degree in civil engineering from Yonsei University in Korea and PhD degree in GIS from University of Wisconsin-Madison in 1998. He was a Director in the Ministry of Construction and Transportation until 2000. He is now a Senior Lecturer of the School of Civil, Urban &

Geosystems Engineering, Seoul National University in Korea.



**Moowook Pyeon** received the BS degree in civil engineering from Seoul National University in Korea and PhD degree in GIS from the same university in 1996. He is now an Assistant Professor of the Department of Civil Engineering, Konkuk University in Korea.